

## Supramolecular Chemistry

How to cite: *Angew. Chem. Int. Ed.* **2023**, *62*, e202300786

International Edition: doi.org/10.1002/anie.202300786

German Edition: doi.org/10.1002/ange.202300786

## Unequal Perylene Diimide Twins in a Quadruple Assembly

Shuqi Chen, Shishi Feng, Albert J. Markvoort,\* Cankun Zhang, Enyang Zhou, WanZhen Liang,\* Hui-Jun Zhang, Yun-Bao Jiang, and Jianbin Lin\*

**Abstract:** Natural light-harvesting (LH) systems can divide identical dyes into unequal aggregate states, thereby achieving intelligent “allocation of labor”. From a synthetic point of view, the construction of such kinds of unequal and integrated systems without the help of proteinaceous scaffolding is challenging. Here, we show that four octatetrayne-bridged *ortho*-perylene diimide (PDI) dyads (**POPs**) self-assemble into a quadruple assembly (**POP**)<sub>4</sub> both in solution and in the solid state. The two identical PDI units in each **POP** are compartmentalized into weakly coupled PDIs (P520) and closely stacked PDIs (P550) in (**POP**)<sub>4</sub>. The two extreme pools of PDI chromophores were unambiguously confirmed by single-crystal X-ray crystallography and NMR spectroscopy. To interpret the formation of the discrete quadruple assembly, we also developed a two-step cooperative model. Quantum-chemical calculations indicate the existence of multiple couplings within and across P520 and P550, which can satisfactorily describe the photophysical properties of the unequal quadruple assembly. This finding is expected to help advance the rational design of dye stacks to emulate functions of natural LH systems.

## Introduction

By recognizing and mimicking how nature plays its parts, we can go far. The self-assembly of  $\pi$ -conjugated molecules by means of noncovalent interactions offers attractive routes toward well-organized functional materials, which helps bridge the gap between natural and artificial systems.<sup>[1]</sup> However, due to the dynamic nature of self-assembly processes, current research in this respect mainly focuses on

isoenergetic aggregates acting in isolation. The constituent  $\pi$ -molecules in the aggregates are equal, which have nearly the same intermolecular packing geometries and coupling strengths.<sup>[2]</sup> Based on a “molecular economy” principle, nature has mastered the art of dividing identical dyes into unequal energy states to accomplish a cooperative task. Because exciton coupling between the same type of chromophores is much stronger than that between different types,<sup>[3]</sup> all the couplings within and across the different energy states render the system of nominally identical dyes fully integrated. For instance, in purple non-sulfur bacterial light-harvesting complex II, twenty-seven identical bacteriochlorophyll *a* (BChl*a*) molecules assemble into two nanorings known as B800 (features nine weakly coupled BChl*a* units) and B850 (consists of eighteen BChl*a* units with a strong *J*-type coupling). Due to the compartmentalization, two kinds of spectrally distinct BChl*a* units can utilize more parts of the solar spectrum and provide a rapid gradient-directed energy transfer from B800 to B850.<sup>[4]</sup> However, without the help of proteinaceous scaffolding, self-assembly of identical dyes into such kind of unequal and integrated systems, especially those with discrete sizes for deriving unambiguous structure–property relationships,<sup>[5]</sup> seems beyond the scope of synthetic chemistry.<sup>[6]</sup>

As an important class of organic dyes with strong  $\pi$ – $\pi$  stacking interactions, perylene diimides (PDIs) have been considered as ideal building blocks for functional supramolecular systems.<sup>[7]</sup> Recently, we are centering our efforts on establishing an equilibrium between enhanced  $\pi$  stacking of *ortho*-modified PDIs<sup>[8]</sup> and growing frustration by steric demand for formation of highly ordered  $\pi$ -aggregates such as discrete stacks<sup>[9]</sup> and alternating stacks.<sup>[10]</sup> In this article, we report that unequal discrete assemblies comprising both weakly coupled and closely stacked dye units can be constructed from covalently connected dye-dye twins (Scheme 1a). We demonstrate that four octatetrayne-

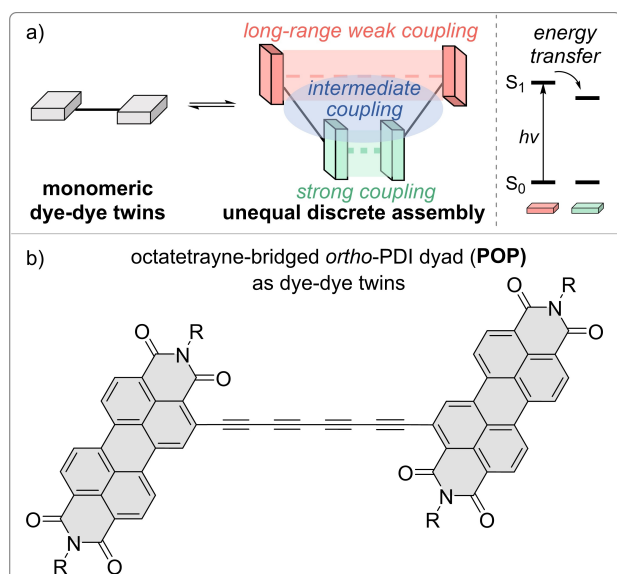
[\*] S. Chen, H.-J. Zhang, Y.-B. Jiang, J. Lin  
Department of Chemistry, College of Chemistry and Chemical Engineering, MOE Key Laboratory of Spectrochemical Analysis and Instrumentation, Xiamen University  
Xiamen 361005 (P. R. China)  
E-mail: jb.lin@xmu.edu.cn

S. Feng, W. Liang  
State Key Laboratory of Physical Chemistry of Solid Surfaces, iChEM, Department of Chemistry, College of Chemistry and Chemical Engineering, Xiamen University  
Xiamen 361005 (P. R. China)  
E-mail: liangwz@xmu.edu.cn

A. J. Markvoort  
Computational Biology Group and Institute for Complex Molecular Systems, Eindhoven University of Technology  
PO Box 513, 5600 MB Eindhoven (The Netherlands)  
E-mail: a.j.markvoort@tue.nl

C. Zhang  
Innovation Laboratory for Sciences and Technologies of Energy Materials of Fujian Province (IKKEM)  
Xiamen 361005 (P. R. China)

E. Zhou  
School of Mathematical Sciences, Xiamen University  
Xiamen 361005 (P. R. China)



**Scheme 1.** a) Schematic illustration of the self-assembly of covalently connected dye-dye twins into an unequal discrete system; b) chemical structure of dye-dye twins **POP** (R = hexylheptyl).

bridged *ortho*-PDI dyads (**POPs**), as the ideal dye-dye twins (Scheme 1b), can entangle with each other through  $\pi$ - $\pi$  interaction and hydrogen bonding, forming a unique quadruple assembly (**(POP)<sub>4</sub>**) both in solution and in the solid state. Eight identical PDI units in four parent **POP** monomers split into two types of PDI aggregates named: P520 (four weakly coupled PDIs) and P550 (two pairs of

closely interacting PDI units). P520 and P550 are named according to their absorption maxima. Within- and cross-couplings of P520 and P550 direct the energy transfer from P520 to P550, which culminates in charge transfer at P550. As a well-defined discrete assembly, (**POP**)<sub>4</sub> can be served as a simple but integrated system to model the light-harvesting process.

## Results and Discussion

### Quadruple assembly in the solid state

Starting from *ortho*-iodinated PDI,<sup>[8c]</sup> **POP** was synthesized through Pd-catalysed Sonogashira coupling (Scheme S1). **POP** displayed good solubility in common organic solvents and was fully characterized by NMR spectroscopy and mass spectrometry. Single crystals suitable for X-ray diffraction analysis were grown by slow diffusion of methanol into a chloroform solution of **POP**.<sup>[11]</sup> Figure 1a shows that the quadruple **POP** assembly (**(POP)<sub>4</sub>**) is spatially isolated by a total of 16 swallow-tail-like hexylheptyl groups that stretch around the assembly to prevent further stacking (Figure 1a,b). In (**POP**)<sub>4</sub>, the substitution at *ortho*-positions of PDI units does not introduce perylene-core twists. Two octatetrayne-bridged PDI units in one **POP** are differentiated by distinct interactions with the neighboring units. Thus, a (**POP**)<sub>4</sub> has two extreme sets of PDI chromophores: P520 (light red) features four quasi-monomeric PDI units isolated by the octatetrayne linkers, whereas P550 (light green) represents two pairs of closely associated PDI units. In P550, the PDI units are stacked as a dimer, exhibiting a

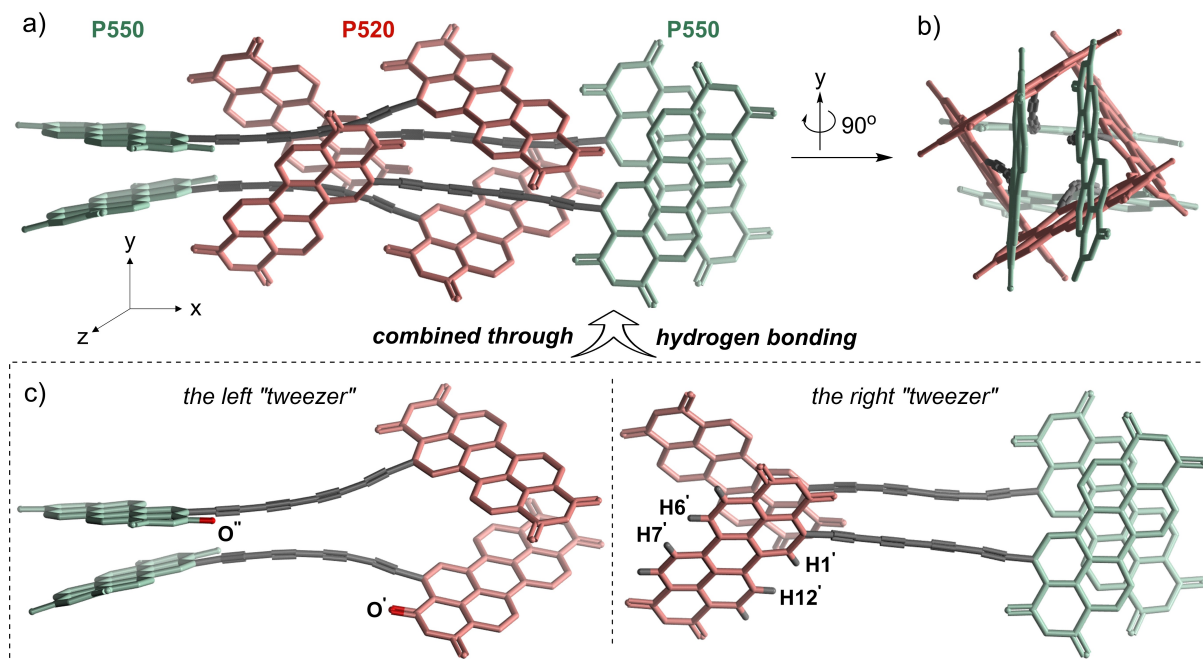


**Figure 1.** (**POP**)<sub>4</sub> in the solid state. a) b) ORTEP structures of (**POP**)<sub>4</sub> (front and side views). c) The left and right parts of (**POP**)<sub>4</sub> showing  $\pi$ - $\pi$  stacking and hydrogen bonding (H6', H7'...O'', H1', H12'...O'). Hexylheptyl groups and hydrogen atoms are omitted for clarity, and only one of the four PDI units in P520 is labeled with hydrogen atoms.



(POP)<sub>4</sub> might proceed at a rate similar to the NMR time scale, and therefore the peaks shown in Figure 2b are broad at 298 K. Further evidence of the dynamic exchange is the appearance of negative signs (yellow, Figure 2e) between protons of PDIs in P520 and P550 at 353 K.

### Two-step cooperative mechanism

The assembly of such discrete systems like (POP)<sub>4</sub> cannot be interpreted by the conventional monomer-dimer or infinite monomer-oligomer systems models.<sup>[13]</sup> As shown in Figure 3a, the formation of (POP)<sub>4</sub> can follow an assembly process via either an isodesmic (path a, all monomer association equilibrium constants  $K_{1-2}$ ,  $K_{2-3}$ , and  $K_{3-4}$  are equal) or a two-step mechanism (path b, dimerizations of monomers with association equilibrium constants  $K_{1-2}$  are followed by coalescence of two dimers with association equilibrium constant  $K_{2-4}$ ;  $K_{1-2} \neq K_{2-4}$ ;  $\sigma = K_{1-2}/K_{2-4}$ ;  $\sigma > 1$ : anti-cooperative growth;  $\sigma < 1$ : cooperative growth). Specific formation of (POP)<sub>4</sub> in MCH solution, as determined by NMR studies, rules out the possibility of an isodesmic mechanism, which would result in a continuous distribution of POP, (POP)<sub>2</sub>, (POP)<sub>3</sub>, and (POP)<sub>4</sub> assemblies. Anti-cooperative growth is also unlikely because an accumulation

of (POP)<sub>2</sub> was not observed. As a result, we propose a cooperative two-step three-state chemical equilibrium (Path b):  $4 \text{ POP} \rightleftharpoons 2 \text{ (POP)}_2 \rightleftharpoons \text{(POP)}_4$ , yielding mass balance equation:

$$c_0 = [\text{POP}] + 2 K_{1-2} [\text{POP}]^2 + 4 K_{2-4} K_{1-2}^2 [\text{POP}]^4 \quad (1)$$

where  $c_0$  refers to the total concentration of POP molecules and [POP] represents the equilibrium concentration of POP monomer.

This equation allows to calculate [POP] as a function of  $c_0$ ,  $K_{1-2}$  and  $K_{2-4}$ , and via  $K_{1-2} = \exp(-(\Delta H_{12} - T\Delta S_{12})/RT)$  and  $\sigma = K_{1-2}/K_{2-4}$  the fraction aggregated ( $\alpha = 1 - [\text{POP}]/c_0$ ) as a function of  $c_0$ , an enthalpy term  $\Delta H_{12}$ , an entropy term  $\Delta S_{12}$  and cooperativity  $\sigma$ . Then, the solution behavior of POP was further studied by concentration and temperature-dependent UV/Vis spectroscopy in MCH. First, we measured the concentration-dependent spectra at 333 K (Figure 3b).<sup>[14]</sup> At low concentration (0.6  $\mu\text{M}$ ), POP displays a typical monomer absorption band for *ortho*-substituted PDI chromophores with a maximum at 522 nm.<sup>[9]</sup> By increasing the concentration, the absorptions at 485 and 522 nm decreased steadily, whereas two new peaks at 500 and 550 nm emerged and increased gradually. As the monomer is excluded to absorb at 560 nm, we used the absorbance at

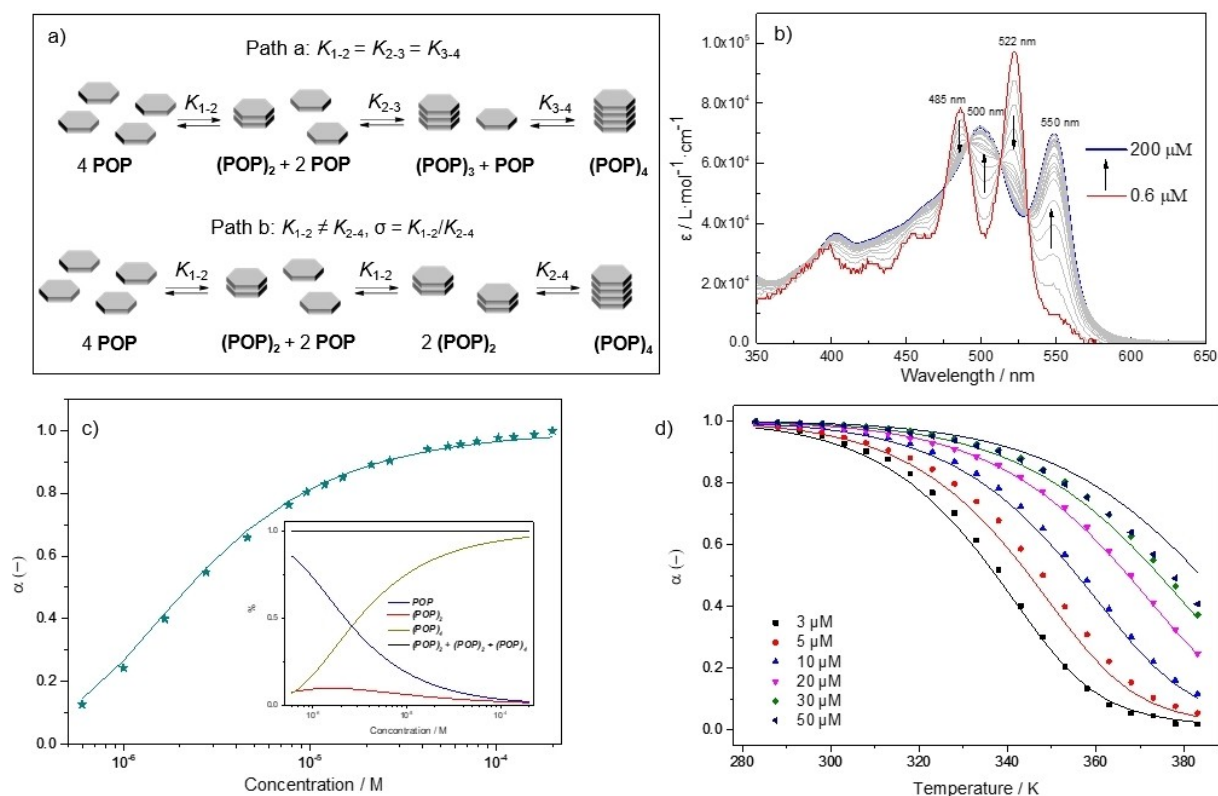


**Figure 3.** a) Schematic illustration of the two models for quadruple assembly (path a: isodesmic model; path b: two-step three-state model). b) Concentration-dependent UV/Vis spectroscopy of POP in MCH at 333 K ( $c_0 = 0.6 - 200 \mu\text{M}$ ). c–d) Fractions aggregated ( $\alpha$ ) versus the overall concentration ( $c_0$ ) at 333 K in part (c) and versus the temperature at a variety of concentrations in part (d). (The data points indicate the fractions derived from the concentration and temperature-dependent UV/Vis adsorption spectra. The lines indicate the prediction of the cooperative two-step model from a fit of all data points combined. The insert in part (c) shows the equilibrium distribution of POP between monomers, dimers (POP)<sub>2</sub>, and tetramers (POP)<sub>4</sub> corresponding to this model fit).

that wavelength to derive the fraction aggregated ( $\alpha$ ) versus the overall concentration ( $c_0$ ) by dividing by the value at 200  $\mu\text{M}$ , resulting in Figure 3c. Next, we also measured the temperature-dependent UV/Vis adsorption at a range of different concentrations, specifically 3  $\mu\text{M}$ , 5  $\mu\text{M}$ , 10  $\mu\text{M}$ , 20  $\mu\text{M}$ , 30  $\mu\text{M}$  and 50  $\mu\text{M}$  (Figure S12). We derived the fractions aggregated (Figure 3d) from the UV/Vis at 540 nm by subtracting the baseline for the lowest concentration and normalizing to the maximum value. Fitting the fractions aggregated derived from the UV/Vis spectra versus concentration (Figure 3c) and the six curves of UV/Vis versus temperature (Figure 3d) collectively to the model predicted fractions (see Supporting Information for details), the best fit was obtained for the two-step model with  $\Delta H_{12} = -65.36 \text{ kJ mol}^{-1}$ ,  $\Delta S_{12} = -0.102 \text{ kJ mol}^{-1}\text{K}$  ( $K_{1-2} = 8.7 \times 10^4 \text{ M}^{-1}$  at 333 K) and  $\sigma = 0.00436$  ( $K_{2-4} = 2.0 \times 10^7 \text{ M}^{-1}$  at 333 K). Although the sum squared residual landscape around this optimum is shallow (Figure S14), implying that the exact value of the cooperativity may deviate, clearly only a sufficiently cooperative model fits the data.<sup>[15]</sup> Note that, cooperative growth of  $\pi$ -systems usually results in much larger aggregates, but not in discrete and well-defined assembly like in this case.<sup>[16]</sup>

### Electronic couplings in $(\text{POP})_4$

Selective constructions of discrete  $\pi$ -stacks with well-defined sizes and aggregation structures are crucial for in-depth studies on structure–property relationships of  $\pi$ -conjugated molecular materials, which can only be realized recently.<sup>[17]</sup> In the quadruple assembly, PDI pools may have diverse electronic couplings, which drive exciton transport and photophysical properties.<sup>[18]</sup> In order to better understand the intermolecular interactions in  $(\text{POP})_4$ , we calculate the electronic couplings between the diabatic states of nine representative dimers shown in Figure 4 and Figure S4: ((P550-1)–(P550-2), (P520-1)–(P520-2), (P550-1)–(P520-3), (P550-2)–(P520-4), (P550-1)–(P520-1), (P550-1)–(P520-4), (P550-2)–(P520-3), (P520-1)–(P520-3), and (P520-2)–(P520-4)). The fragment particle–hole densities (FPHD) diabaticization method<sup>[19]</sup> is adopted to construct the various quasi-diabatic states via the linear combinations of the adiabatic ones, which are calculated by time-dependent density functional theory (TDDFT) with exchange–correlation functional CAM-B3LYP and basis set 6-311G(d,p). Because the alkyl chains at imide positions hardly affect the electronic structure of PDI, to save the computational cost, we simplify the crystal structure of the  $(\text{POP})_4$  by replacing the hexylheptyl groups with isopropyl groups in the following calculations. For a PDI monomer, TDA-CAM-B3LYP produces two well-separated lowest-lying singlet excited states with excitation energies of 2.740 and 3.631 eV. For each dimer, we thus only consider the four lowest-lying singlet diabatic states: two localized excited (LE) states and two intermolecular charge transfer (CT) states, indicating that the high-energy LE and CT states are neglected in the later calculations. As Figure 4b–e shows, the LE states and CT states can be distinguished based on the electron and

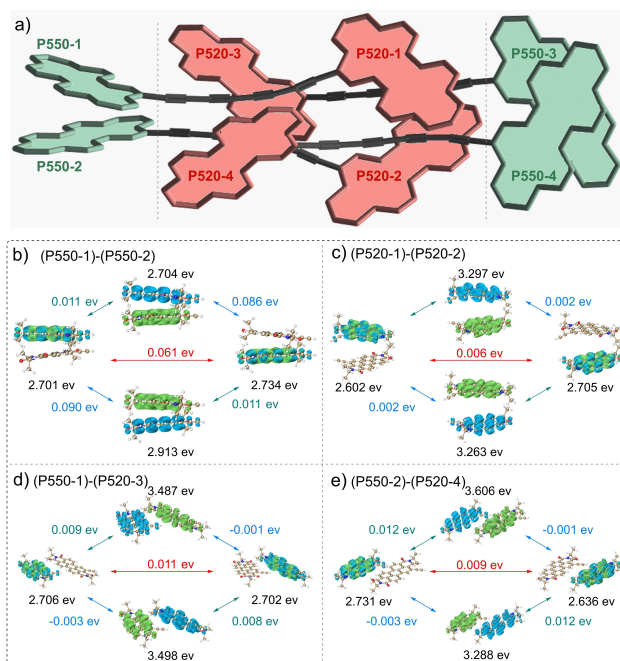


**Figure 4.** a) Structure of the  $(\text{POP})_4$  with labeling of the constituent PDI units. b–e) Diabatic results of four different PDI dimers in the  $(\text{POP})_4$  assembly. (Hexylheptyl groups have been replaced by isopropyl groups to simplify the calculations, the red, green, and blue double arrows present the excitonic couplings, hole, and electron-transfer integrals, respectively. The blue and green isosurfaces with an isovalue of 0.001 a.u. correspond to the electron and hole wavefunction distributions. Coupling values less than 0.001 eV are omitted.)

hole wavefunction distributions that the LE states correspond to the electron and hole wavefunction localized on the same molecular fragment whereas the CT states correspond to the electron and hole wavefunction distributed on the two adjacent molecules, respectively. It is observed that for P550 the calculated excitonic coupling is 0.061 eV and the electron and hole transfer integrals are 0.090 and 0.011 eV, respectively. These values being are much larger than those in the other nearest-neighboring dimers, suggests that P550 plays the most significant role both in the excitation energy transfer and charge transfer processes in  $(\text{POP})_4$ . The excitonic couplings in the other three PDI dimers ((P520-1)–(P520-2), (P550-1)–(P520-3), (P550-2)–(P520-4)) are ca. 6, 11, and 9 meV, respectively. Therefore, the energy transfer processes are likely to come out partly in these three PDI dimers after photoexcitation. The exciton dissociation processes from the LE states to the CT states may arise in the (P550-1)–(P520-3) and (P550-2)–(P520-4) dimers via the hole transfer process according to the magnitude of the coupling value. However, the energy of the CT state in the (P550-1)–(P520-3) and (P550-2)–(P520-4) dimers are much higher than that of the LE state. Therefore, the exciton dissociation processes are rather difficult to take place in the P520–P550 dimers in  $(\text{POP})_4$ .

Based on those diabatic results, we calculate the vibrationally-resolved absorption spectra of  $(\text{POP})_4$  by using the non-Markovian stochastic Schrödinger equations.<sup>[20]</sup> Fig-

ure 5a shows that the calculated spectrum of P550 agrees well with the experimental spectrum of  $(\text{POP})_4$  in the low-energy absorption region while the absorption of P520 is similar to that of a  $\text{POP}$  monomer, which further confirms the above analysis that the P550 makes the dominant contribution to the photophysical properties of  $(\text{POP})_4$ . Therefore, we focus on analyzing the spectral characteristics of P550 instead of the entire  $(\text{POP})_4$ .

In Figure S5, we show the effects of the CT states and vibrational motions on the two absorption peaks based on the P550 configuration. By comparing the spectral features with and without the contributions of CT states and vibrational motions, we confirm that the two main low-energy absorption peaks with a spacy separation of 53 nm and nearly identical intensities come from the strong mixing of LE and CT states. The remarkable influences of the CT states and vibrational motions result in pronounced bathochromic shifts of the lowest-energy absorption band compared to that of the monomer.

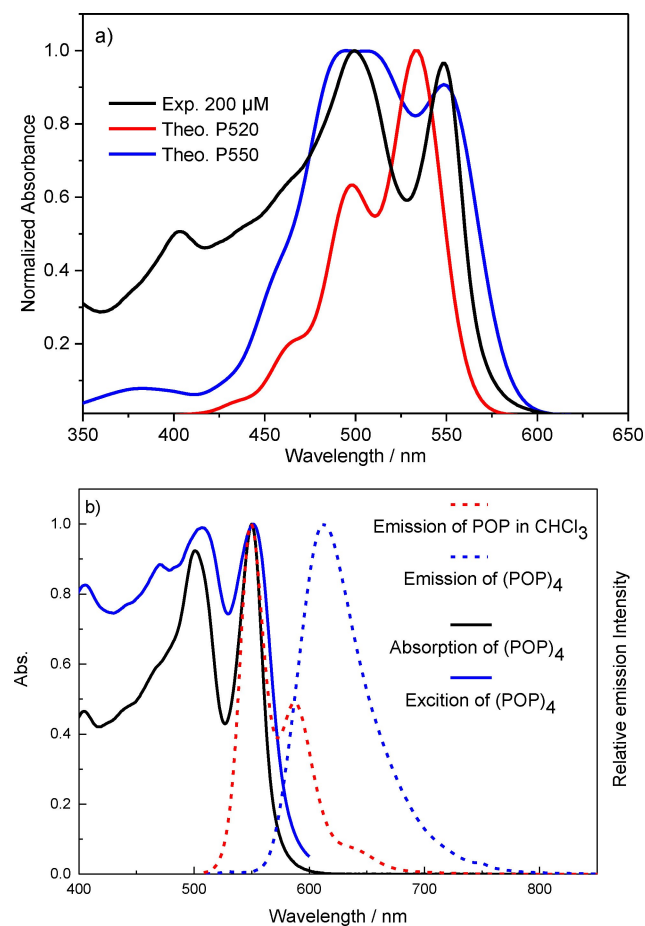


**Figure 5.** a) Vibrationally resolved absorption spectra of P520 and P550 in  $(\text{POP})_4$ . The black solid line represents the experimental measurement. To compare with the experimental result, the calculated spectra are all red-shifted by 0.304 eV. b) Normalized absorption spectrum (black solid line) and normalized excitation spectrum (blue solid line, monitoring the emission intensity at 610 nm) of  $(\text{POP})_4$  and emission spectra (dashed lines, Ex. = 490, 500 nm, respectively) of  $\text{POP}$  (red) and  $(\text{POP})_4$  (blue). ( $\text{POP}$  = 50  $\mu\text{M}$ , 298 K).

The important roles of CT states have been reported by many researchers.<sup>[7b,18, 21]</sup> These roles are closely related to exciton dissociation, charge separation,<sup>[22]</sup> and singlet fission.<sup>[23]</sup> In addition, vibrational motions may facilitate ultrafast symmetry-breaking charge separation processes, which have been proposed in PDI systems.<sup>[24]</sup> These results encouraged us to further investigate the photophysical properties of  $(\text{POP})_4$  using spectroscopic techniques.

### Modelling light harvesting with $(\text{POP})_4$

According to the theoretical investigation, the absorption spectrum of  $(\text{POP})_4$  can be considered as a summation of the spectra of P550 and P520. As shown in Figure 5b, the emission of  $\text{POP}$  monomer in dichloromethane is observed at 550 nm with a low fluorescence quantum yield of 2.2 % and a lifetime of 120 ps. A rotation around the octatetrayne axis is probably a reason for the accelerated fluorescence decay compared to those of general PDI derivatives.  $(\text{POP})_4$  in MCH shows emission at 613 nm with a low quantum yield of 2.4 % and a lifetime of 1.1 ns (Figure S6), typical of the excimer emission of P550. The emission of P520 completely disappeared. Moreover, the excitation spectrum of the excimer emission is in reasonable agreement with the absorption spectrum of  $(\text{POP})_4$ , the sum of the spectra of P550 and P520, indicating that the interactions between the PDI units essentially provide a gradient that directs energy flow from P520 to P550.<sup>[25,26]</sup>

Figure S7a shows the transient absorption (TA) spectrum of  $(\text{POP})_4$  in MCH, which displays a rapid decay of excited singlet state absorption at 700 nm and a concomitant growth of two new absorption bands at around 580 and 820 nm. The new bands are attributed to  $\text{PDI}^{\bullet+}$  (580 nm) and  $\text{PDI}^{\bullet-}$  (820 nm) by comparison to the absorption spectra of PDI radical cation and anion from both control experiments (Figure S7b) and previous literature.<sup>[27]</sup>

### Conclusion

The present study shows that the construction of novel unequal discrete assemblies is achievable with dye-dye twins. The quadruple assembly  $(\text{POP})_4$  featuring two extreme pools of PDI units (P520 and P550) is unambiguously confirmed in both the solid state and solution. High binding constants ( $K_{1,2} = 8.7 \times 10^4 \text{ M}^{-1}$  and  $K_{2,4} = 2.0 \times 10^7 \text{ M}^{-1}$  at 333 K) are determined based on a two-step cooperative model. Spectroscopic studies indicate that, following photoexcitation, energy is transferred from P520 to P550, culminating in charge transfer to P550. Thus, within- and cross-couplings of P520 and P550 make  $(\text{POP})_4$  a simple but integrated model system to capture, transfer, and convert solar energy. As a proof of concept, this work displays that self-assembly of identical dyes into fully integrated molecular artificial systems is feasible, yielding optimal supramolecular model systems to investigate complex phenomena such as “quantum coherence”.<sup>[28]</sup>

## Acknowledgements

We are grateful for financial support from the Natural Science Foundation of China (No. 22071208, 22171237, 22271239, 21833006, 22173074), the Youth Innovation foundation of Xiamen (3502Z20206058), and the Natural Science Foundation of Fujian Province (2022J01524).

## Conflict of Interest

The authors declare no conflict of interest.

## Data Availability Statement

The data that support the findings of this study are available in the Supporting Information of this article.

**Keywords:** Coupling · Discrete Stacking · Light Harvesting · Perylene Diimide · Unequal Assembly

- [1] a) T. Aida, E. W. Meijer, S. I. Stupp, *Science* **2012**, *335*, 813–817; b) Z. Chen, A. Lohr, C. R. Saha-Moller, F. Würthner, *Chem. Soc. Rev.* **2009**, *38*, 564–584; c) F. J. M. Hoeben, P. Jonkheijm, E. W. Meijer, A. Schenning, *Chem. Rev.* **2005**, *105*, 1491–1546.
- [2] a) D. Bialas, E. Kirchner, M. I. S. Rohr, F. Würthner, *J. Am. Chem. Soc.* **2021**, *143*, 4500–4518; b) F. C. Spano, *Acc. Chem. Res.* **2010**, *43*, 429–439.
- [3] D. Bialas, A. Zitzler-Kunkel, E. Kirchner, D. Schmidt, F. Würthner, *Nat. Commun.* **2016**, *7*, 12949.
- [4] a) T. Mirkovic, E. E. Ostroumov, J. M. Anna, R. van Grondelle, Govindjee, G. D. Scholes, *Chem. Rev.* **2017**, *117*, 249–293; b) T. Brixner, R. Hildner, J. Köhler, C. Lambert, F. Würthner, *Adv. Energy Mater.* **2017**, *7*, 1700236; c) R. Croce, H. van Amerongen, *Nat. Chem. Biol.* **2014**, *10*, 492–501.
- [5] N. Aratani, D. Kim, A. Osuka, *Acc. Chem. Res.* **2009**, *42*, 1922–1934.
- [6] a) S. Sengupta, F. Würthner, *Acc. Chem. Res.* **2013**, *46*, 2498–2512; b) P. D. Frischmann, K. Mahata, F. Würthner, *Chem. Soc. Rev.* **2013**, *42*, 1847–1870; c) J. Yang, M.-C. Yoon, H. Yoo, P. Kim, D. Kim, *Chem. Soc. Rev.* **2012**, *41*, 4808–4826; d) M. R. Wasielewski, *Acc. Chem. Res.* **2009**, *42*, 1910–1921; e) M. R. Wasielewski, *J. Org. Chem.* **2006**, *71*, 5051–5066; f) B. Rybtchinski, L. E. Sinks, M. R. Wasielewski, *J. Am. Chem. Soc.* **2004**, *126*, 12268–12269.
- [7] a) M. Hecht, F. Würthner, *Acc. Chem. Res.* **2021**, *54*, 642–653; b) R. M. Young, M. R. Wasielewski, *Acc. Chem. Res.* **2020**, *53*, 1957–1968; c) F. Würthner, C. R. Saha-Möller, B. Fimmel, S. Ogi, P. Leowanawat, D. Schmidt, *Chem. Rev.* **2016**, *116*, 962–1052; d) M. Sun, K. Mullen, M. Yin, *Chem. Soc. Rev.* **2016**, *45*, 1513–1528; e) S. Chen, P. Slattum, C. Wang, L. Zang, *Chem. Rev.* **2015**, *115*, 11967–11998; f) W. Jiang, Y. Li, Z. Wang, *Acc. Chem. Res.* **2014**, *47*, 3135–3147.
- [8] a) L. Zhang, I. Song, J. Ahn, M. Han, M. Linares, M. Surin, H.-J. Zhang, J. H. Oh, J. Lin, *Nat. Commun.* **2021**, *12*, 142; b) F. Su, S. Chen, X. Mo, K. Wu, J. Wu, W. Lin, Z. Lin, J. Lin, H.-J. Zhang, T.-B. Wen, *Chem. Sci.* **2020**, *11*, 1503–1509; c) J. Wu, D. He, L. Zhang, Y. Liu, X. Mo, J. Lin, H. J. Zhang, *Org. Lett.* **2017**, *19*, 5438–5441.
- [9] F. Su, G. Chen, P. A. Korevaar, F. Pan, H. Liu, Z. Guo, A. Schenning, H. J. Zhang, J. Lin, Y. B. Jiang, *Angew. Chem. Int. Ed.* **2019**, *58*, 15273–15277; *Angew. Chem.* **2019**, *131*, 15417–15421.
- [10] H. Li, P. Shao, S. Chen, G. Li, X. Feng, X. Chen, H. J. Zhang, J. Lin, Y. B. Jiang, *J. Am. Chem. Soc.* **2020**, *142*, 3712–3717.
- [11] Deposition number 2203453 (for (POP)<sub>4</sub>) contains the supplementary crystallographic data for this paper. These data are provided free of charge by the joint Cambridge Crystallographic Data Centre and Fachinformationszentrum Karlsruhe Access Structures service.
- [12] G. R. Desiraju, *Acc. Chem. Res.* **1996**, *29*, 441–449.
- [13] a) J. Gerschberg, F. Fennel, T. H. Rehm, S. Lochbrunner, F. Würthner, *Chem. Sci.* **2016**, *7*, 1729–1737; b) M. M. J. Smulders, M. M. L. Nieuwenhuizen, T. F. A. de Greef, P. van der Schoot, A. P. H. J. Schenning, E. W. Meijer, *Chem. Eur. J.* **2010**, *16*, 362–367; c) T. F. De Greef, M. M. Smulders, M. Wolffs, A. P. Schenning, R. P. Sijbesma, E. W. Meijer, *Chem. Rev.* **2009**, *109*, 5687–5754.
- [14] At room temperature in MCH, subtle changes in the concentration-dependent UV/Vis spectroscopy of POP prove to be very challenging for further analysis.
- [15] Fitting the concentration dependent curve together with the 6 temperature dependent curves to 1) the isodesmic model yielded the fits as in Figures S17 and S18. Clearly, the isodesmic model does not fit as well as the two-step model; 2) the dimer model yielded the fits as in Figures S20 and S21. Clearly, the dimer model does not fit the data properly either..
- [16] C. Kulkarni, E. W. Meijer, A. R. A. Palmans, *Acc. Chem. Res.* **2017**, *50*, 1928–1936.
- [17] a) G. Wu, F. Li, B. Tang, X. Zhang, *J. Am. Chem. Soc.* **2022**, *144*, 14962–14975; b) M. Mahl, M. A. Niyas, K. Shoyama, F. Würthner, *Nat. Chem.* **2022**, *14*, 457–462; c) X. Hu, J. O. Lindner, F. Würthner, *J. Am. Chem. Soc.* **2020**, *142*, 3321–3325; d) E. Kirchner, D. Bialas, F. Fennel, M. Grune, F. Würthner, *J. Am. Chem. Soc.* **2019**, *141*, 7428–7438; e) C. Kaufmann, W. Kim, A. Nowak-Krol, Y. Hong, D. Kim, F. Würthner, *J. Am. Chem. Soc.* **2018**, *140*, 4253–4258; f) C. Shao, M. Stolte, F. Würthner, *Angew. Chem. Int. Ed.* **2013**, *52*, 7482–7486; *Angew. Chem.* **2013**, *125*, 7630–7634.
- [18] N. J. Hestand, F. C. Spano, *Acc. Chem. Res.* **2017**, *50*, 341–350.
- [19] Y.-C. Wang, S. Feng, W. Z. Liang, Y. Zhao, *J. Phys. Chem. Lett.* **2021**, *12*, 1032–1039.
- [20] Y.-C. Wang, Y. Ke, Y. Zhao, *WIREs Comput. Mol. Sci.* **2019**, *9*, e1375.
- [21] a) Y. Hong, J. Kim, W. Kim, C. Kaufmann, H. Kim, F. Würthner, D. Kim, *J. Am. Chem. Soc.* **2020**, *142*, 7845–7857; b) N. J. Hestand, F. C. Spano, *Chem. Rev.* **2018**, *118*, 7069–7163.
- [22] H. Tamura, I. Burghardt, *J. Am. Chem. Soc.* **2013**, *135*, 16364–16367.
- [23] a) Y. Hong, M. Rudolf, M. Kim, J. Kim, T. Schembri, A.-M. Krause, K. Shoyama, D. Bialas, M. I. S. Röhr, T. Joo, H. Kim, D. Kim, F. Würthner, *Nat. Commun.* **2022**, *13*, 4488; b) L. Wang, W. Cai, J. Sun, Y. Wu, B. Zhang, X. Tian, S. Guo, W. Z. Liang, H. Fu, J. Yao, *J. Phys. Chem. Lett.* **2021**, *12*, 12276–12282.
- [24] a) C. Lin, T. Kim, J. D. Schultz, R. M. Young, M. R. Wasielewski, *Nat. Chem.* **2022**, *14*, 786–793; b) Y. Hong, F. Schlosser, W. Kim, F. Würthner, D. Kim, *J. Am. Chem. Soc.* **2022**, *144*, 15539–15548; c) T. Kim, C. Lin, J. D. Schultz, R. M. Young, M. R. Wasielewski, *J. Am. Chem. Soc.* **2022**, *144*, 11386–11396.
- [25] a) Y. Wang, H. Chen, H. Wu, X. Li, Y. Weng, *J. Am. Chem. Soc.* **2009**, *131*, 30–31; b) T. H. Brotsudarmo, R. Kunz, P. Böhm, A. T. Gardiner, V. Moulisová, R. J. Cogdell, J. Köhler, *Biophys. J.* **2009**, *97*, 1491–1500; c) L. Stryer, R. P. Haugland, *Proc. Natl. Acad. Sci. USA* **1967**, *58*, 719–726.
- [26] The coupling between P520 and P550 ( $\approx 10$  meV) may allow for coherent energy transfer on ultrashort (fs) time scales,

which cannot be resolved by conventional time-resolved spectroscopy. For references, see: E. Collini, G. D. Scholes, *Science* **2009**, 323, 369–373.

- [27] a) J. Kong, W. Zhang, G. Li, D. Huo, Y. Guo, X. Niu, Y. Wan, B. Tang, A. Xia, *J. Phys. Chem. Lett.* **2020**, 11, 10329–10339;  
b) J. Sung, A. Nowak-Król, F. Schlosser, B. Fimmel, W. Kim, D. Kim, F. Würthner, *J. Am. Chem. Soc.* **2016**, 138, 9029–9032.
- [28] G. D. Scholes, G. R. Fleming, L. X. Chen, A. Aspuru-Guzik, A. Buchleitner, D. F. Coker, G. S. Engel, R. van Grondelle, A.

Ishizaki, D. M. Jonas, J. S. Lundeen, J. K. McCusker, S. Mukamel, J. P. Ogilvie, A. Olaya-Castro, M. A. Ratner, F. C. Spano, K. B. Whaley, X. Zhu, *Nature* **2017**, 543, 647–656.

Manuscript received: January 16, 2023

Accepted manuscript online: February 15, 2023

Version of record online: March 2, 2023